ARTICLES
PUBLISHED ONLINE: 30 NOVEMBER 2015 | DOI: 10.1038/NCLIMATE2877
nature climate change

Making methane visible

Magnus Gålfalk[1]*, Göran Olofsson[2], Patrick Crill[3] and David Bastviken[1]

Methane (CH_4) is one of the most important greenhouse gases, and an important energy carrier in biogas and natural gas. Its large-scale emission patterns have been unpredictable and the source and sink distributions are poorly constrained. Remote assessment of CH_4 with high sensitivity at a m^2 spatial resolution would allow detailed mapping of the near-ground distribution and anthropogenic sources in landscapes but has hitherto not been possible. Here we show that CH_4 gradients can be imaged on the $<m^2$ scale at ambient levels (~1.8 ppm) and filmed using optimized infrared (IR) hyperspectral imaging. Our approach allows both spectroscopic confirmation and quantification for all pixels in an imaged scene simultaneously. It also has the ability to map fluxes for dynamic scenes. This approach to mapping boundary layer CH_4 offers a unique potential way to improve knowledge about greenhouse gases in landscapes and a step towards resolving source–sink attribution and scaling issues.

Identifying sources and sinks of CH_4 and comparing their relative magnitudes in landscapes is challenging but important. CH_4 is the second most important greenhouse gas at a 100-year perspective[1] and has a high value for society as an energy source. Atmospheric levels of CH_4 have increased 2.5-fold since 1750 (ref. 1) but the reasons for this increase are not as clear as for carbon dioxide (CO_2). For example, although atmospheric CO_2 levels have increased steadily, the accumulation rate of CH_4 has varied for unknown reasons[2]. Suggested explanations that are based on the balance of emissions from fossil fuels and wetlands[2] are difficult to verify and alternative explanations cannot be excluded because sources and sinks are too poorly constrained.

CH_4 is produced by methanogenic archaea in anaerobic systems including sediments and water-saturated soils, gastrointestinal systems of animals, biogas production and waste management systems[2,3]. CH_4 is also released from natural gas handling and combustion processes[2]. The major sinks are believed to be atmospheric oxidation and microbial oxidation in soils, sediments, and water[2,3]. Wetland plants, or bubbling through shallow inland waters, function as gas conduits from anaerobic sediments. Similarly, there are also hot spot sources in agriculture (for example, rice paddies, waste lagoons, and ruminants), and industrial and urban environments (combustion and gas distribution leaks). Many if not most large sources, both natural and anthropogenic, are confined to local sites with a patchy distribution across landscapes. The sinks may also be scattered in the landscape on the basis of, for example, local moisture levels in soils. Because of the difficulty in quantitatively assessing the spatial variability of sources and sinks our current knowledge is probably biased and incomplete.

A fundamental limitation in our ability to identify and compare CH_4 sources and sinks is related to the spatial scales of available measurement techniques. Bottom-up methods often rely on flux chamber or point concentration measurements. Flux chamber measurements have a well-defined but very small footprint (typically sub-m^2) and cannot easily be used to cover larger areas. High-frequency measurements can be obtained by eddy covariance (EC) and gradient-based flux assessments with larger footprints at ha to km^2 scales (ref. 4), but specific sources and sinks within the footprint cannot be resolved. EC and gradient flux footprints are based on statistical probability distributions, vary over time, and lack verifiable boundaries. A less common approach is the backward Lagrangian stochastic (bLs) technique[5] which uses a laser and a reflector for each line of sight and can be used to locate a point source (or several sources depending on the number of lines of sight used) or estimate emission rates through dispersion model predictions. The dispersion models also have footprint uncertainties and specific infrastructure is required for each line of sight (such as the laser source and reflector), which limits the spatial distribution of the measurements.

Several satellites have been or are now mapping CH_4 on a global to regional scale, including SCIAMACHY (ref. 6), GOSAT (ref. 7), AIRS (ref. 8), IASI/AMSU (ref. 9), and the planned CarbonSat (ref. 10) and GRIPS (ref. 11), all having km-scale spatial resolutions. Satellites are very useful for their spatial coverage and have been successfully used in many projects for following regional patterns[12–15], but two drawbacks are the low spatial resolution and difficulties in resolving CH_4 at the surface–atmosphere boundary layer where the source/sink patterns are revealed. A recent example is the four corners CH_4 hotspot, a 6,500 km^2 coal mining area in the US emitting enough CH_4 to be seen from space but still measuring only a few pixels in SCIAMACHY images[16]. Although successfully mapping atmospheric CH_4 content, the large pixel sizes limit our ability to link CH_4 levels to environmental drivers that may differ between different types of environments/land use. Remote sensing of CH_4 from aircraft is also in development. Examples are AirGRIPS (gas-filter correlation radiometer) and the MaMap spectrometer[17], giving a resolution of 33 × 23 m at 1,000 m altitude. Higher-resolution (several m^2) measurements of strong CH_4 sources have been made in both the shortwave[18,19] and thermal IR (ref. 20) from high altitudes, representing important progress. However, a technique with the ability to map lower levels of near-ground CH_4 in landscapes at very high spatial resolution (sub-m^2), having a high enough spectral resolution to ensure separation of CH_4 from other gases, yet with good spatial and temporal coverage, and the ability to measure flow velocities directly from high-speed imaging, would substantially increase our capacity to identify,

[1]Department of Thematic Studies—Environmental Change, Linköping University, 581 83 Linköping, Sweden. [2]Department of Astronomy, Stockholm University, 106 91 Stockholm, Sweden. [3]Department of Geological Sciences, Stockholm University, 106 91 Stockholm, Sweden.
*e-mail: magnus.galfalk@liu.se

Table 1 | Summary of our flux measurements made in different case study environments, including fluxes from both diffuse and point sources.

Scene	Temp. contrast (°C)	Flow tracking (Hz)	CH_4 flux from camera	Comparison with independent measurements for the same system (IMSS) or literature data from similar systems
Controlled release 1				IMSS*
10 cubes, 4.3 min avg.	5–15	245	$25.3 \pm 2.8\ g\ h^{-1}$	$23 \pm 2.3\ g\ h^{-1}$
Controlled release 2				IMSS*
10 cubes, 4.3 min avg.	5–15	245	$102.9 \pm 5.8\ g\ h^{-1}$	$100 \pm 10\ g\ h^{-1}$
Cows in a barn			$160 \pm 5\ g\ h^{-1}$	Literature review[21]
16 cubes, 26.4 min avg.	9	64	$77.8 \pm 2.1\ kg\ yr^{-1}\ cow^{-1}$	67.5–98.6 $kg\ yr^{-1}\ cow^{-1}$
Cows in a barn			$154 \pm 25\ g\ h^{-1}$	Literature review[21]
16 cubes × 99 s	9	64	$75 \pm 12\ kg\ yr^{-1}\ cow^{-1}$	67.5–98.6 $kg\ yr^{-1}\ cow^{-1}$
Waste incineration			$696 \pm 38\ g\ h^{-1}$	IMSS†
40 cubes, 14.3 min avg.	24	473	$6.1 \pm 0.33\ t\ yr^{-1}$	$<9.5\ t\ yr^{-1}$ (30 min mean)
				$<4.7\ t\ yr^{-1}$ (daily mean)
Sewage sludge deposit				Sludge treatment wetlands[25]‡
7 cubes × 40 s	1–2	155	102 (0–560) $mg\ m^{-2}\ h^{-1}$	10–5,400 $mg\ m^{-2}\ h^{-1}$
				Dry sewage sludge[26]‡
				0–6,381 $mg\ m^{-2}\ h^{-1}$

For comparison, fluxes measured with alternative techniques in similar environments are also provided. *Manual bubble flux measurements; this study. †Point measurements in smoke were made by incineration plant staff during a different time period, large variability and uncertainty in measurements (data from the yearly environmental report[27] from the company running the plant). ‡There is a large small-scale heterogeneity in fluxes from sludge depending on treatment and local moisture. Previous measurements based on point measurements and enclosures may therefore have an unknown bias and may not be directly comparable to our flux integrating over a large area and not interfering with the sludge surface and air movement around the deposit.

resolve, and compare different sources and sinks. In turn, this would lead to new possibilities for understanding the variability of CH_4 in the atmosphere, detecting and minimizing CH_4 leakage or emissions from anthropogenic processes, and also validating how environmental change (for example, land-use and climate change) affect CH_4 source attribution in climate models. We here present a new and generally applicable technique based on thermal IR hyperspectral imaging for landscapes that does not require a priori knowledge of source localization.

Imaging methane on a landscape scale

Hyperspectral imaging can be described as imaging that records a spectrum for each pixel simultaneously in a scene. Thereby a three-dimensional data cube is generated for each imaging sequence with two dimensions defining the scene spatially and a third dimension holding the spectral information (Supplementary Fig. 1). In the thermal IR part of the electromagnetic spectrum this is often a passive technique with patterns of absorption or emission lines, depending on whether the background is hotter or colder than the gas (the temperature contrast). Those patterns can be used as fingerprints of individual chemical compounds in the line of sight, making assessment of concentration gradients possible (Supplementary Fig. 2).

Our hyperspectral camera, described in the Supplementary Methods, was developed for optimized detection of CH_4 (7.7 μm band) allowing more sensitive quantification of concentration gradients than were previously avilable. Using all the spectra in a data cube and spectroscopic radiative transfer modelling at a high spectral resolution (0.25 or $1\ cm^{-1}$) a time-averaged CH_4 image can be calculated pixel-by-pixel (described in Supplementary Methods). The high imaging frequency of the camera during data acquisition (images including all spectral lines) also made it possible to separately derive air motion from H_2O and CH_4 motion and to construct air flow movies. In cases with high enough CH_4 fluxes and low humidity the CH_4 can be followed directly, while water vapour can be used as the air flow tracer in other cases. The presented technique can therefore generate sensitive static spectra by aggregating information over the image collection time (0.25–2 min per cube) to detect and measure the average amount of CH_4 with high precision, as well as construct air flow movies. By combining the gradients in CH_4 levels quantified from spectra with the information about net air movement, corresponding average CH_4 fluxes during the image collection period can then be assessed. Thus not only concentration gradients but also fluxes can be calculated from the obtained images and spectra for both hot-spot and diffuse emission sources.

After testing the system extensively in the lab, several successful field measurements were made. Below we present CH_4 images of different environments to demonstrate the ability of the system to remotely map CH_4 at ambient levels (~1.8 ppm; parts per million by volume) under field conditions (typically a few °C background-gas temperature contrast). We highlight examples of CH_4 mapping, showing the ability to map concentration gradients, find emission hot-spots in the landscape, and quantify CH_4 fluxes. A summary of the scenes and measured CH_4 fluxes are given in Table 1, including a comparison with typical fluxes found in the literature where available. *In situ* measurements for comparisons were also made using an infrared Off-Axis Integrated Cavity Output Spectroscopy (OA-ICOS) greenhouse gas analyser (Los Gatos Research, DLT 100 or UGGA).

Controlled gas release

The first example shows a controlled release of CH_4 on the lawn outside our lab (Fig. 1) at $45\ ml\ s^{-1}$ ($100 \pm 10\ g\ h^{-1}$; measured manually with a volumetric bubble flow meter). The spectroscopically calculated CH_4 image was made from one cube (200 × 90 pixels at $1\ cm^{-1}$ spectral resolution) and shows our CH_4 source and its surrounding average distribution (Fig. 1a). The air–background temperature contrast was found from the spectra to be in the range of 5–15 °C (air 19 °C, and the wall 24–34 °C) with a background distance of 50 m. By relating the mapped CH_4 from spectroscopy with the air flow from the large number of individual IR images collected over time during the imaging (in this scene 245 Hz, 6,320 images in 25.8 s) we could quantify and follow the CH_4 flow at a high temporal resolution (Fig. 1b and Supplementary Movie 1). Using 10 cubes, a spectroscopically modelled average CH_4 distribution, and detailed high-frequency imaging of the CH_4 motion (wind speeds 0.1–0.3 $m\ s^{-1}$) we calculated a flux of

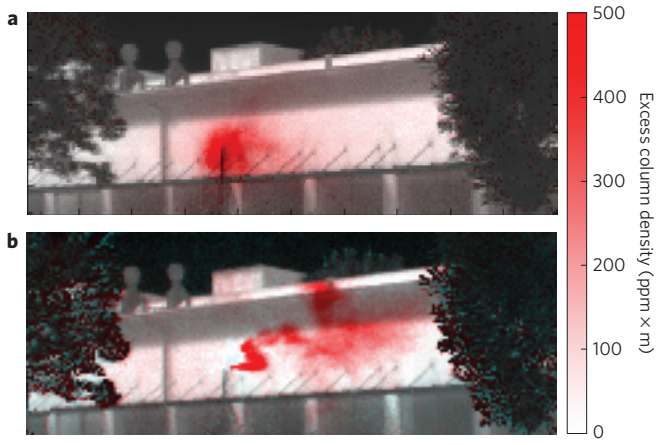

Figure 1 | Outdoor detection and quantification of controlled CH_4 release. Column densities of CH_4 above the ambient level are shown using different shades of red, overlaid on a thermal IR image. **a**, Average distribution (one cube, acquisition time 25.8 s). **b**, Snapshot (40 out of 6,320 images in the cube, integration time 0.16 s).

Figure 2 | Image of CH_4-rich air vented from a barn with 18 cows inside (one cube, acquisition time 99 s). The multilayered spectroscopic model gives CH_4 column densities (red) above the ambient level in the outlet flow. Crosses 1 and 2 mark locations for the example spectra in Fig. 3, and cross 3 marks the position where *in situ* measurements were made for validation.

$102.9 \pm 5.8\,g\,h^{-1}$. For a second test with a smaller release of $10\,ml\,s^{-1}$ (measured to $23 \pm 2.3\,g\,h^{-1}$ by the volumetric gas flow meter) and higher wind speeds ($0.8–2.7\,m\,s^{-1}$) we calculated a flux of $25.3 \pm 2.8\,g\,h^{-1}$ using data from the camera. Thus, these controlled fluxes could be accurately determined with the camera.

Cows in a barn

The second example is a barn with 18 cows inside. A plume of CH_4- rich air from the ventilation outlet was clearly revealed in our spectroscopic CH_4 image (Fig. 2), representing the average flow. The temperature difference was 9 °C between the plume and the background wall. The spectroscopic modelling (see Supplementary Methods) uses four layers: reflected cold sky off the building, heat radiation from the building itself (−1 to +1 °C), the plume (+8.8 °C at the outlet), and a layer of cold air between the plume and the camera (−2.9 °C) that contains CH_4 and H_2O at air temperature. Example spectra (spectral resolution $1\,cm^{-1}$) used for quantification of CH_4 within and outside the vent plume (points 1 and 2 in Fig. 2) are shown (Fig. 3) together with the corresponding spectroscopic model fits. *In situ* measurements in the outlet flow (location 3 in Fig. 2) of 15 ppm are in agreement with our column measurements (∼30 ppm m/2 m thick plume = ∼15 ppm). The imaging frequency of the camera in this scene was 63.8 Hz (6,320 images in 99 s, 320 × 256 pixels), with a high enough signal-to-noise ratio (S/N) to follow the flow at a high temporal resolution (Supplementary Movie 2). From structures in the plume, the flow speed was found to be $1.02\,m\,s^{-1}$ and combined with concentration and flux data generated over 26 min (16 cubes) our models gave a CH_4 flux of $43\,mg\,s^{-1}$ ($160 \pm 5\,g\,h^{-1}$). This is equivalent to $77.8 \pm 2.1\,kg\,yr^{-1}$ cow^{-1} if a constant flux is assumed. In a recent review[21] it was stated that a cow emits 67.5–98.6 kg $CH_4\,yr^{-1}$, depending on grazing, in agreement with our measurements.

Waste incineration plant

As another example of the detection and quantification of anthropogenic CH_4 emissions, we mapped the chimney exhaust of a waste incineration plant (Fig. 4) using a previously published method for obtaining chimney mass flow rates[22,23], with the cold sky as the background and a spectral resolution of $0.25\,cm^{-1}$ from a distance of 183 m. The cold sky had a radiation temperature between −55 °C and the air temperature (8.5 °C) depending on the wavelength and zenith angle, and the gas plume had an average temperature of +32.9 °C close to the outlet (measured from its water content, compensating for the CH_4 content in the air in front of and behind the plume). Three layers were used in the data modelling (cold sky, hot plume, and cold air in the foreground). The vertical flow velocity in the plume ($2.50\,m\,s^{-1}$) was measured from flow structures using the IR images collected at a rate of 473 Hz. The average wind speed of $1.9\,m\,s^{-1}$ did not affect flow velocity estimates as the flow velocity is still vertical close to the chimney. With information on both the average CH_4 column density profile and the flow velocity in the plume using 40 cubes (14.3 min), a CH_4 flux of $696 \pm 38\,g\,h^{-1}$ could be calculated, corresponding to $6.1 \pm 0.33\,t\,y^{-1}$ if a constant flux is assumed. Such stand-off flux assessments could represent a breakthrough in cases such as this, where accurate flux measurements can be difficult to perform with traditional methods. It should also be noted that CH_4 fluxes from incineration or industrial combustion processes are often neglected or considered to be negligible[24], while our measurements showed that this is not the case.

Sewage sludge deposit

As an example of mapping CH_4 gradients and fluxes in a scene with temperature differences less than a few °C and low–medium concentrations (ambient ∼2 ppm to ∼10 ppm mixing ratios) we mapped CH_4 around a sewage sludge deposit (Fig. 5). The regions shown as dark red in the lower part of the image have the highest mixing ratios because the lines of sight are directly towards the sludge deposit, while lower average mixing ratios are found along the lines of sight further up in the map, almost reaching the ambient level towards the distant trees (the ambient level was found by measuring a scene in a different direction that was unaffected by the deposits). The average wind speed was $1.7\,m\,s^{-1}$ from left to right in Fig. 5. *In situ* point measurements over the nearby edge of the sludge deposit showed a mixing ratio of 8 ppm above ambient, which is in agreement with the mixing ratios in the CH_4 map (∼7 ppm; Fig. 5; note that some deviation between point measurements and integrated line-of-sight values from the camera is expected). The map was made from 16 cubes (320 × 100 pixels) with a spectral resolution of $1\,cm^{-1}$. Using seven cubes (40.6 s acquisition time per cube) we applied mass balance calculations in a 3.7 × 17 m ($62\,m^2$) region of the sludge area, with air motions tracked from our high-frequency imaging and CH_4 column densities from the corresponding spectroscopy, to estimate the average CH_4 emission to be $102\,mg\,m^{-2}\,h^{-1}$ ($0.89\,kg\,m^{-2}\,yr^{-1}$) with estimates for each cube in the range $0–560\,mg\,m^{-2}\,h^{-1}$. Fluxes from sludge treatment are

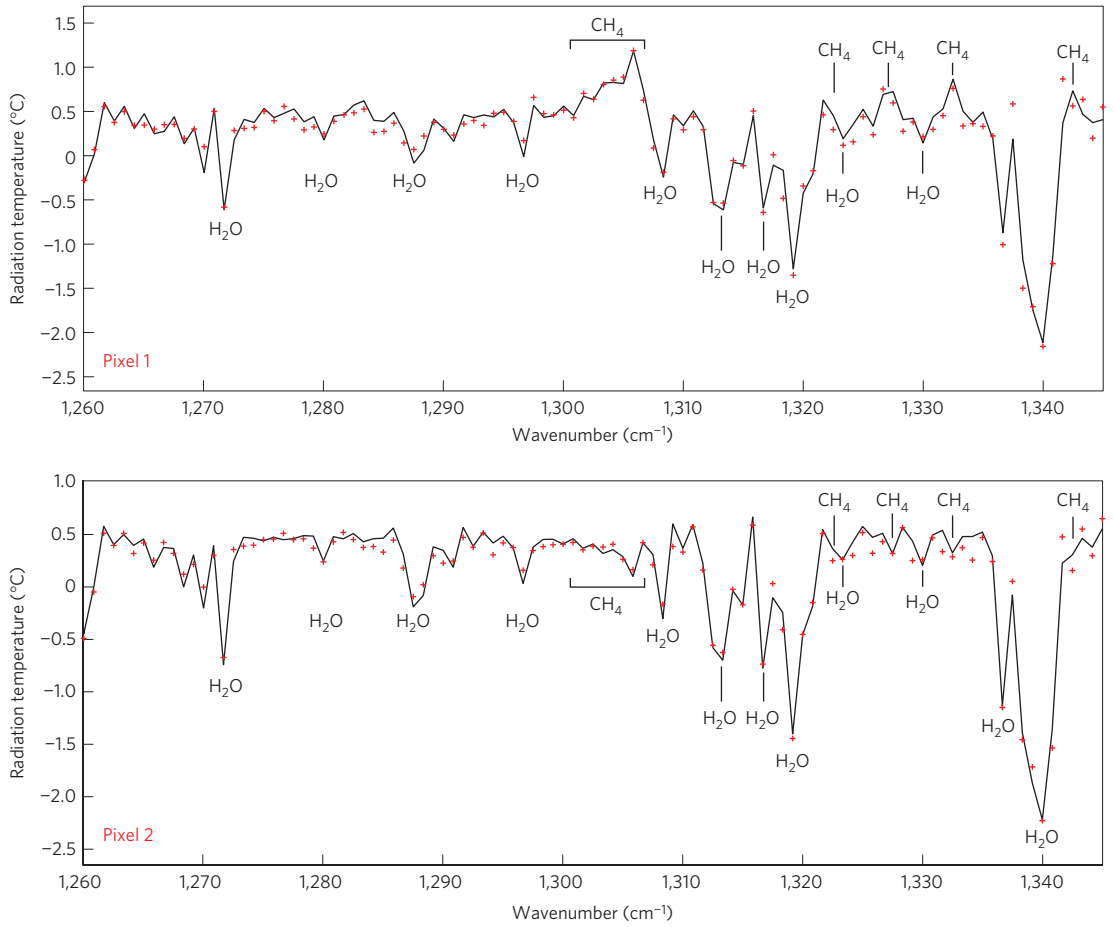

Figure 3 | Spectra of pixels in and outside of the barn outflow (Fig. 2). Red crosses represent measurement points and solid curves the corresponding models. The spectral resolution was 1 cm^{-1}. Warm CH_4 is clearly detected in the flow pixel as emission lines (top panel), while only a small amount of cold CH_4 (ambient concentration between wall and camera) is seen as absorption lines in the pixel outside the flow (bottom panel).

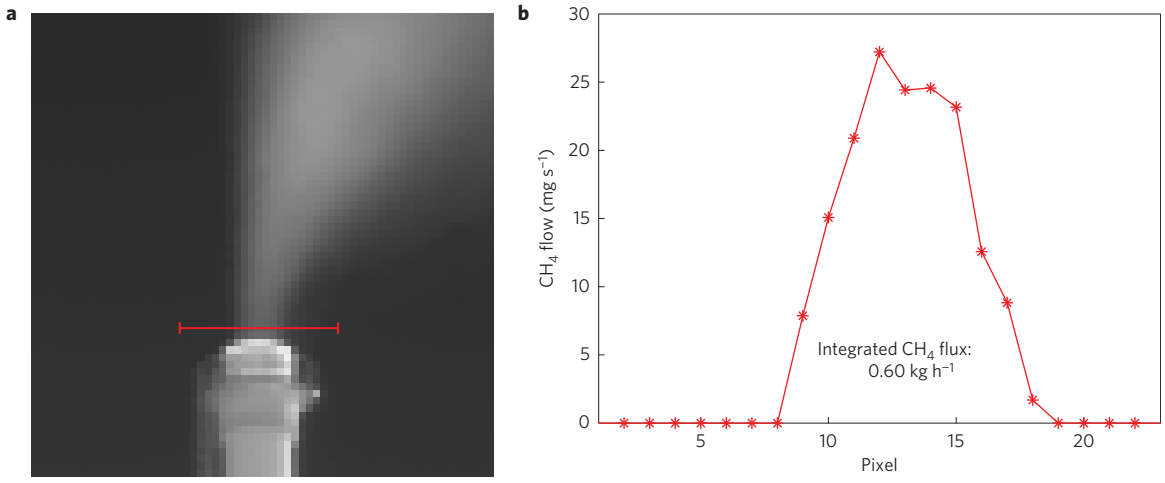

Figure 4 | Imaging of CH_4 flowing from a waste incineration plant chimney (40 cubes, acquisition time 14.3 min). a, Thermal image of chimney and plume (mostly H_2O) with the cross-section in **b** marked by a red line. **b**, Measured CH_4 flux in the cross section and the total flux.

known to be highly variable depending on the type of treatment and the age of the material. Literature values for sludge treatment wetlands based on traditional methods are often in the range 10–5,400 mg m^{-2} h^{-1} (ref. 25). Fluxes from sewage sludge can reach from 0 to above 6,300 mg m^{-2} h^{-1} depending on the age and surface moisture of the sludge, with high spatial variability on deposits being frequently observed[26]. All of our measurements confirm the high spatial variability and are within the ranges reported previously, but cross comparisons with other traditional techniques should be made with care and not always focus on correspondence. This type of remote assessment, not disturbing the studied system, being based on direct spectroscopic detection of gas concentration

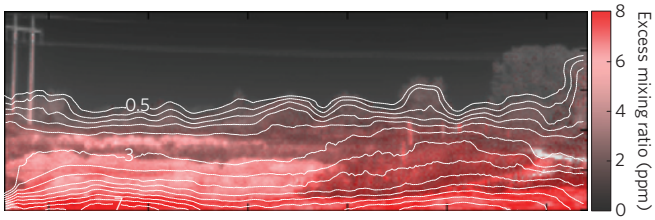

Figure 5 | Map of CH_4 release from a sewage sludge deposit (24 cubes, acquisition time 16.3 min). Thermal IR image with excess (above ambient) average CH_4 mixing ratios along each line of sight (pixel) overlaid as red colours and as a contour map. The contours are at 0.5 ppm intervals in the range 0.5–7 ppm.

gradients as well as direct assessment of detailed undisturbed air motion, and ability to integrate over large areas yet having a well-defined measurement footprint, may be more likely to return accurate fluxes than methods based on, for example, small-scale enclosures/chambers disturbing the air motion that contributes to fluxes, and possibly affecting the underlying sludge near the chamber edges.

Discussion

Altogether the presented system and related image analyses were capable of visualizing and quantifying CH_4 levels, and in many cases also associated fluxes, from widely different types of sources and under varying conditions. A discussion on the uncertainties of the method is given in the Supplementary Methods, together with an example of CH_4 mapping at ambient levels above an oligotropic boreal lake.

An overview of the examples provided above and other previous remote sensing techniques capable of detecting CH_4 that we are aware of is provided in Supplementary Table 1 (see Supplementary Methods for an overview of differences between remote sensing approaches). The approach presented here seems to be in the order of 40 and 100 times more sensitive for concentrations and flux assessments, respectively, while at the same time having a higher spectral and spatial resolution, yielding more robust separation of CH_4 from other gases. Thus, our approach opens up new opportunities for imaging of CH_4 concentration gradients and hot spots at a high spatial resolution with measurements made from the ground, or from above using a helicopter at an altitude of up to several hundred metres. It thereby seems highly suitable for mapping both natural and anthropogenic sources and potentially also sinks (see Supplementary Fig. 4) without any a priori knowledge of their distribution in a given scene.

Received 17 September 2014; accepted 13 October 2015; published online 30 November 2015

References

1. IPCC *Climate Change 2013: The Physical Science Basis* (eds Stocker, T. F. *et al.*) (Cambridge Univ. Press, 2013).
2. Kirschke, S. *et al.* Three decades of global methane sources and sinks. *Nature Geosci.* **6,** 813–823 (2013).
3. Reeburgh, W. S. in *Treatise on Geochemistry* Vol. 4 (ed. Keeling, R.) 65–89 (Elsevier, 2003).
4. Denmead, O. T. Approaches to measuring fluxes of methane and nitrous oxide between landscapes and the atmosphere. *Plant Soil* **309,** 5–24 (2008).
5. Flesch, T. K. *et al.* Multi-source emission determination using an inverse-dispersion technique. *Bound. Layer Meteorol.* **132,** 11–30 (2009).
6. Frankenberg, C. *et al.* Global column-averaged methane mixing ratios from 2003 to 2009 as derived from SCIAMACHY: trends and variability. *J. Geophys. Res.* **116,** D04302 (2011).
7. Bril, A. *et al.* Retrievals of atmospheric CO_2, CH_4 and optical path modifications from the GOSAT observations. *Proc. SPIE* **8890,** 889008 (2013).
8. Xiong, X. *et al.* Seven years' observation of mid-upper tropospheric methane from atmospheric infrared sounder. *Remote Sens.* **2,** 2509–2530 (2010).
9. Crevoisier, C. *et al.* Tropospheric methane in the tropics—first year from IASI hyperspectral infrared observations. *Atmos. Chem. Phys.* **9,** 6337–6350 (2009).
10. Buchwitz, M. *et al.* Carbon monitoring satellite (CarbonSat): assessment of atmospheric CO_2 and CH_4 retrieval errors by error parameterization. *Atmos. Meas. Tech.* **6,** 3477–3500 (2013).
11. Schoeberl, M. *et al.* The geostationary remote infrared pollution sounder (GRIPS): Measurement of the carbon gases from space. *Proc. SPIE* **8866,** 886602 (2013).
12. Beck, V. *et al.* Methane airborne measurements and comparison to global models during BARCA. *J. Geophys. Res.* **117,** D15310 (2012).
13. Bergamaschi, P. *et al.* Inverse modeling of global and regional CH_4 emissions using SCIAMACHY satellite retrievals. *J. Geophys. Res.* **114,** D22301 (2009).
14. Schneising, O. *et al.* Three years of greenhouse gas column-averaged dry air mole fractions retrieved from satellite—Part 2: Methane. *Atmos. Chem. Phys.* **9,** 443–465 (2009).
15. Worden, J. *et al.* CH_4 and CO distributions over tropical fires during October 2006 as observed by the Aura TES satellite instrument and modeled by GEOS-Chem. *Atmos. Chem. Phys.* **13,** 3679–3692 (2013).
16. Satellite data shows U.S. Methane 'hot spot' bigger than expected. *NASA News* (9 October 2014); http://www.nasa.gov/press/2014/october/satellite-data-shows-us-methane-hot-spot-bigger-than-expected
17. Gerilowski, K. *et al.* MAMAP—a new spectrometer system for column-averaged methane and carbon dioxide observations from aircraft: Instrument description and performance analysis. *Atmos. Meas. Tech.* **4,** 215–243 (2011).
18. Roberts, D. A. *et al.* Mapping methane emissions from a marine geological seep source using imaging spectrometry. *Remote Sens. Environ.* **114,** 592–606 (2010).
19. Thorpe, A. K. *et al.* High resolution mapping of methane emissions from marine and terrestrial sources using a Cluster-Tuned Matched Filter technique and imaging spectrometry. *Remote Sens. Environ.* **134,** 305–318 (2013).
20. Tratt, D. M. *et al.* Airborne visualization and quantification of discrete methane sources in the environment. *Remote Sens. Environ.* **154,** 74–88 (2014).
21. Cottle, D. J., Nolan, J. V. & Wiedemann, S. G. Ruminant enteric methane mitigation: A review. *Anim. Prod. Sci.* **51,** 491–514 (2011).
22. Tremblay, P. Standoff gas identification and quantification from turbulent stack plumes with an imaging Fourier-transform spectrometer. *Proc. SPIE* **7673,** 76730H (2010).
23. Savary, S. Standoff identification and quantification of flare emissions using infrared hyperspectral imaging. *Proc. SPIE* **8024,** 880240T (2011).
24. Astrup, T. *et al.* Incineration and co-combustion of waste: Accounting of greenhouse gases and global warming contributions. *Waste Manag. Res.* **27,** 789–799 (2009).
25. Uggetti, E. *et al.* Quantification of greenhouse gas emissions from sludge treatment wetlands. *Wat. Resour.* **46,** 1755–1762 (2012).
26. Flodman, M. *Emissioner av Metan, Lustgas och Ammoniak vid Lagring av Avvattnat Rötslam* (*Emissions of Methane, Nitrous Oxide and Ammonia during Storage of Dewatered Sludge*) MSc thesis, Swedish Univ. Agricultural Sciences (2002).
27. *Tekniska Verken Environmental Report* (Tekniska Verken, 2013); https://www.tekniskaverken.se/contentassets/4d1aac7dc84c40ee9d25099d40c05325/2013-miljorapport-garstadverket-29425.pdf

Acknowledgements

This study was funded by an instrument grant from the Knut and Alice Wallenberg Foundation (ref no. KAW 2010.0126) to the authors and by a grant from the Swedish Research Council VR to D.B. (ref. no. VR 2012-48). We thank the camera production team at Telops Quebec City, Canada, for their great interest, for committing exceptional expertise in the hardware development, and for invaluable support. We also thank H. Reyier (Linköping University) for practical assistance and P. Falkenström and R. Sahlée for help with accessing measurement locations.

Author contributions

G.O. generated the initial idea which was developed together with D.B., M.G., and P.C. D.B. led the fundraising with help from M.G., P.C. and G.O. M.G. led the practical imaging work, performed image analyses, and made the spectroscopic and radiative transfer models. M.G. and D.B. led the writing of the paper, with all authors contributing to manuscript development.

Additional information

Supplementary information is available in the online version of the paper. Reprints and permissions information is available online at www.nature.com/reprints. Correspondence and requests for materials should be addressed to M.G.

Competing financial interests

The authors declare no competing financial interests.